




RESEARCH ARTICLE

Degradation of Ge subcells by thermal load during the growth of multijunction solar cells

Enrique Barrigón^{1,2*}  | Mario Ochoa^{1*}  | Ivan García¹  | Laura Barrutia¹  | Carlos Algara¹  | Ignacio Rey-Stolle¹ 

¹Instituto de Energía Solar, Universidad Politécnica de Madrid, Avda Complutense 30, 28040 Madrid, Spain

²Solid State Physics, Department of Physics and NanoLund, Lund University, Box 118, 221 00 Lund, Sweden

Correspondence

Enrique Barrigón, Instituto de Energía Solar, Universidad Politécnica de Madrid, Avda Complutense 30, 28040 Madrid, Spain.
Email: enrique.barrigon@ies-def.upm.es

Funding information

European Commission, Grant/Award Number: 607153

Abstract

Germanium solar cells are used as bottom subcells in many multijunction solar cell designs. The question remains whether the thermal load originated by the growth of the upper layers of the multijunction solar cell structure affects the Ge subcell performance. Here, we report and analyze the performance degradation of the Ge subcell due to such thermal load in lattice-matched GaInP/Ga(In)As/Ge triple-junction solar cells. Specifically, we have detected a quantum efficiency loss in the wavelength region corresponding to the emitter layer (which accounts for up to 20% loss in equivalent J_{SC}) and up to 55 mV loss in V_{OC} of the Ge subcell as compared with analogous devices grown as single-junction Ge solar cells on the same type of substrates. We prove experimentally that there is no direct correlation between the loss in V_{OC} and the doping level of the base. Our simulations show that both the J_{SC} and V_{OC} losses are consistent with a degradation of the minority carrier properties at the emitter, in particular at the initial nanometers of the emitter next to the emitter/window heterointerface. In addition, we also rule out the gradual emitter profile shape as the origin of the degradation observed. Our findings underscore the potential to obtain higher efficiencies in Ge-based multijunction solar cells if strategies to mitigate the impact of the thermal load are taken into consideration.

KEYWORDS

Ge solar cells, multijunction solar cells, thermal degradation, thermal load

1 | INTRODUCTION

Nowadays, III to V based multijunction solar cells (MJSCs) exhibit the highest conversion efficiencies of any photovoltaic device.¹ Multijunction solar cells consist of a variety of subcells made of different materials and electrically interconnected. Typically, Ge is the preferred material to be used as the bottom subcell (BC) in a MJSC because, among others, (i) it shows a low energy bandgap (E_g); (ii) it can be employed as the mechanical support of the stack (ie, Ge wafers are relatively inexpensive and widely available); and (iii) it is compatible with the subsequent growth of an extensive family of III-V compounds (ie, subcells with different bandgaps can be grown on it with high quality). One drawback of this material is its lower potential to achieve high conversion efficiency as compared with direct

III-V semiconductors. Therefore, understanding and optimizing its performance is important to take full advantage of Ge subcells in MJSC.

The most widespread MJSC design based on Ge is the lattice-matched GaInP/Ga(In)As/Ge triple junction solar cell (3JSC) with record efficiencies in excess of 40%.² In this device, the Ge BC is highly current mismatched (with respect to the GaInP top and Ga(In)As middle cells, MCs) and exhibits a relatively low V_{OC} . For the typical terrestrial or space solar spectra, the Ge BC produces excess photocurrent with respect to the other 2 subcells, and thus, it will never limit the photocurrent of a well-designed lattice-matched 3JSC and it contributes to enhance the efficiency of the 3JSC (with respect to a GaInP/GaAs 2JSC case) by the voltage added by the bottom junction. Therefore, this voltage should be maximized. In other current-matched MJSC configurations (eg, 4JSC), the Ge bottom cell may limit the photocurrent generated by the MJSC, and therefore, its external quantum efficiency (EQE) should be also maximized.³

*These authors contributed equally to this work.

The copyright line for this article was changed on 24 April 2018 after original online publication.

This is an open access article under the terms of the Creative Commons Attribution License, which permits use, distribution and reproduction in any medium, provided the original work is properly cited.

© 2017 The Authors. *Progress in Photovoltaics: Research and Applications* Published by John Wiley & Sons Ltd.

Multijunction solar cells are generally grown by metal organic vapor phase epitaxy. Unlike all the III-V layers forming the MJSC structure, the Ge BC is created by the in-diffusion of group V elements (n-type dopants in Ge) during the growth of the first III-V layers on the p-type Ge substrate (the so-called nucleation layer⁴). Thus, the nucleation layer must be optimized not only considering the epi-surface morphology^{5,6} but also from the point of view of the Ge subcell emitter formation. Indeed, Friedman and Olson reported that for a Ge solar cell with a base doping of $1 \cdot 10^{18} \text{ cm}^{-3}$, the V_{OC} is limited by the properties of the emitter.⁷ In particular, to obtain a high V_{OC} , the emitter should exhibit (i) a low emitter surface-recombination velocity (S_E), (ii) a reduced thickness (X_E), and (iii) a high minority carrier diffusion length ($L_{n,E}$, where h stands for holes and E for emitter). Krut and coworkers⁸ also showed that the performance of Ge subcells is enhanced with reduced emitter thickness. Typical materials for the nucleation layer on Ge(100) include GaAs^{9,10} or GaInP,^{5,6} yielding in both cases a good template for the subsequent MJSC growth. However, the use of GaInP is preferred as it creates a shallower emitter than GaAs because the solubility and diffusion coefficients of P in Ge are higher and lower, respectively, than that of As.^{11,12}

In any case, after its formation, the Ge subcell suffers the thermal load associated with the growth of the rest of the subcells forming the MJSC structure (sometimes referred to as “thermal load” for brevity in this text). In this line, Gudovskikh and coworkers¹³ reported the formation of a potential barrier at the n-GaInP/n-Ge heterointerface, due to the simultaneous diffusion of group III elements (Ga and In) into the Ge substrate.

Here, we report on the degradation of the performance at 1 sun of the Ge subcell due to the thermal load suffered in a 3JSC. Although this work is only focused on the GaInP/Ga(In)As/Ge 3JSC, the degradation observed and its mechanisms may also apply to other MJSC configurations such as upright metamorphic MJSCs¹⁴ or other MJSCs with 4 or 5 junctions grown on Ge.^{3,15}

2 | EXPERIMENTAL AND MODELLING

Germanium single-junction solar cell structures were grown in a commercial Aixtron 200/4 metal organic vapor phase epitaxy reactor on p-type gallium doped Ge(100) wafers with 6° misorientation to the [111]. The semiconductor structure of the *as-grown* devices can be seen in Figure 1. By *as-grown* we mean the solar cell that results after growing the semiconductor structure shown in Figure 1. A GaInP nucleation layer on Ge was employed, which also acted as the window layer of the Ge solar cell. A Ga(In)As cap layer was grown on top to facilitate the formation of ohmic contacts. Two different growth temperatures (640 and 675°C)

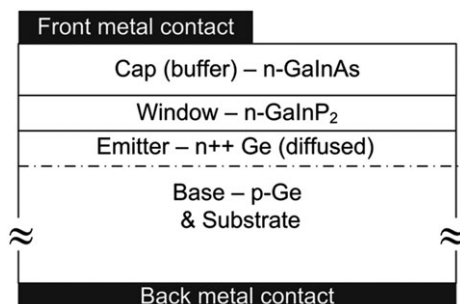


FIGURE 1 Structure of the Ge solar cells analyzed in this work

were used to grow these III-V layers, to test their effects on the emitter formation and its performance, and the growth time was around 45 minutes in all cases. Details on the growth can be found elsewhere.⁴

Triple junction solar cell solar cells were also grown by using the same nucleation conditions (materials, growth temperature, and Ge wafer resistivity). Table 1 includes information about the growth temperatures and time employed during the growth of the 3JSCs, and more generic details about these 3JSC structures can be found elsewhere.¹⁶ Subsequently, the GaInP top cell (TC), Ga(In)As MC, and tunnel junctions were chemically etched away and the samples were processed into solar cells, using the GaInAs buffer layer as the cap layer. In this way, the assessment of the effect of the thermal load of the growth of the rest of the subcells forming the 3JSC structure on the Ge BC performance is straightforward by comparison with the *as-grown* solar cells of Figure 1. Hereafter, these Ge solar cells will be referred to as *etched 3JSC* devices. A summary of all the structures analyzed in this work can be found in Table 1, where “#A” and “#E” stand for *as-grown* and *etched 3JSC*, respectively. As can be observed in Table 1, a set of Ge wafers with different resistivities were used to study the effect of this variable on the performance of the Ge subcells. Although the reader may be more familiar with carrier concentration values, we prefer to use resistivity values instead because they are generally employed by Ge wafer manufacturers and the resistivity measurement of the epiwafers is straightforward and more reliable than the value extracted from electrochemical capacitance-voltage (C-V) measurements performed from the front of the n on p structures. As a reference to the reader, the carrier concentration value range explored covers approximately from 4×10^{17} to $4 \times 10^{18} \text{ cm}^{-3}$.

Several solar cells were manufactured with an active area of 0.1156 cm^2 by using standard photolithography techniques and gold electroplating for the formation of the metal contacts. In the *etched* devices, front metal contacts were made on the Ga(In)As cap layer (see Figure 1) after etching. No antireflection coating (ARC) was deposited on the devices.

Solar cell EQE measurements were taken by using a custom-built, monochromator-based setup with a tungsten lamp as the light source and a monitor detector to compensate for known instabilities in the lamp. A Peltier element with a high-precision controller was used to ensure a constant temperature of 25°C in the solar cell. The system is equipped with a calibrated detector to measure the reflectance (R) in the devices and calculate the internal quantum efficiency (IQE).

Light J-V curves were taken at 25°C by using an X_E lamp-based solar simulator, with a temperature controlled chuck. The simulator is adjusted at the equivalent 1-sun AM1.5d solar spectrum for each cell measured, using reference cells and calculating the spectral mismatch factor. For dark J-V measurements, the same setup was used, but with the lamp shutter closed. Ambient light was prevented from reaching the cells by means of an enclosure that totally covers the measurement setup.

Capacitance-voltage etch-depth profiling was employed to measure the electrical doping and thickness of the diffused emitter. The emitter thickness (X_E) was taken to be equal to the depth of the first p-type point measured with the C-V profile. Secondary-ion mass spectroscopy (SIMS) measurements were also carried out to quantify the concentration of diffused species in the Ge.

Simulations of the device performance and band diagrams were performed with Silvaco Atlas TCAD modeling tool.¹⁷ This type of

TABLE 1 Summary of the growth conditions of the structures under study together with the J_{SC} , V_{OC} , and FF of the resulting devices

Name	Wafer Resistivity ($m\Omega \cdot cm$)	Nucleation Growth T ($^{\circ}C$)	Middle Cell Growth	Top Cell Growth	J_{SC} (mA/cm^2)	V_{OC} (mV)	FF (%)
#A1	6.8	640	N/A	N/A	18.6 (2.1%)	235 (0.3%)	65 (1.4%)
#A2	8.8	640	N/A	N/A	20.4 (1.8%)	244 (0.3%)	66 (1.9%)
#A3	9.5	675	N/A	N/A	18.9 (1.6%)	212 (0.9%)	64.3 (0.8%)
#A4	12.0	640	N/A	N/A	20.6 (1.6%)	241 (0.7%)	66.1 (0.9%)
#E1	8.9	675	75 min @ $640^{\circ}C$	37 min @ $665^{\circ}C$	16.6 (5.4%)	160 (6.1%)	42 (10.4%)
#E2	9.5	640	65 min @ $640^{\circ}C$	23 min @ $640^{\circ}C$	15.4 (2%)	189 (0.8%)	54 (7.4%)
#E3	20.0	675	85 min @ $640^{\circ}C$	23 min @ $675^{\circ}C$	16.9 (2.1%)	180 (0.3%)	60.5 (0.6%)
#E4	22.0	675	75 min @ $640^{\circ}C$	20 min @ $665^{\circ}C$	18.1 (0.9%)	182 (0.4%)	59.9 (1.3%)

A thin tunnel junction was grown at $550^{\circ}C$ before each subcell. The solar cell I to V parameters are averaged values from all measured devices. The relative standard deviation is shown inside brackets.

modeling solves the semiconductor fundamental equations under specified bias conditions.¹⁷ The photogeneration rate has been calculated by using the transfer matrix method,¹⁷ and thermionic and thermionic field emission boundary conditions were used to model the nonlinear transport at heterojunctions. Real doping profiles of the Ge subcells are also included in the simulations. A simultaneous fitting of the EQE, R, and dark and light J-V experimental data is completed to validate the models and material parameters and thus analyze the physical changes behind the degradation. More details about the modeling approach can be found elsewhere.¹⁸

3 | RESULTS

Throughout this section, the results of the different characterization techniques applied to the as-grown and etched 3JSC Ge solar cells are going to be shown in the same figures, while their descriptions are going to be presented separately in the following 2 subsections to facilitate the reading of the paper.

3.1 | As-grown solar cell characterization

Figure 2A shows the IQE of representative as-grown Ge solar cells on substrates with different resistivity values as indicated in Table 1. The

IQE was extracted from the EQE and R measurements of devices with no ARC layer. The IQE reaches values well in excess of 90% from 900 to 1500 nm, which indicates an almost ideal carrier collection in the solar cell. In general, all solar cells show a similar result, with the exception of the structure grown at $675^{\circ}C$ (#A3), which shows a slightly lower IQE. The small differences observed in the wavelength range from 400 to 900 nm are due to different optical thickness (ie, both thickness and composition) of the GaInP window layer and the Ga(In) As contact layer.

The same devices shown in Figure 2A were measured in a solar simulator under 1 sun irradiance. Figure 3 shows as an example the J-V curve of a typical device from structure #A3. In brief, the J-V curve shows a J_{SC} of $19.1 mA/cm^2$, a V_{OC} of 213 mV, and a fill factor (FF) of 65%. A summary of averaged J_{SC} , V_{OC} , and FF values of several devices of each sample can be found in Table 1. Regarding the V_{OC} and the FF, these values agree with reported values of state-of-the-art Ge solar cells.⁷

Figure 4 shows a representative dark J-V curve of the as-grown solar cell with the highest V_{OC} (#A2). The dashed lines indicate the behavior of the current for ideality factors of 1 and 2. The dark J-V curve shows 2 different regions, namely, 1 region with a constant slope (with a kT behavior) and another region dominated by the presence of a high series resistance, corresponding to the bending of the curve at

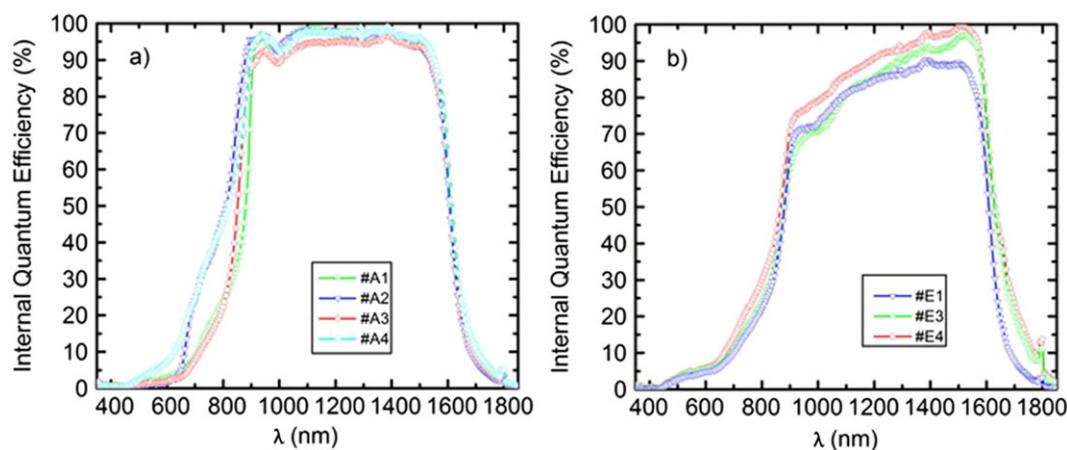


FIGURE 2 Internal quantum efficiency (IQE) of as-grown (A) and etched 3JSC (B) Ge solar cells grown on Ge substrates with different resistivity values. The IQE of #E2 is not included due to its bad morphology, which affects its reflectivity measurement [Colour figure can be viewed at wileyonlinelibrary.com]

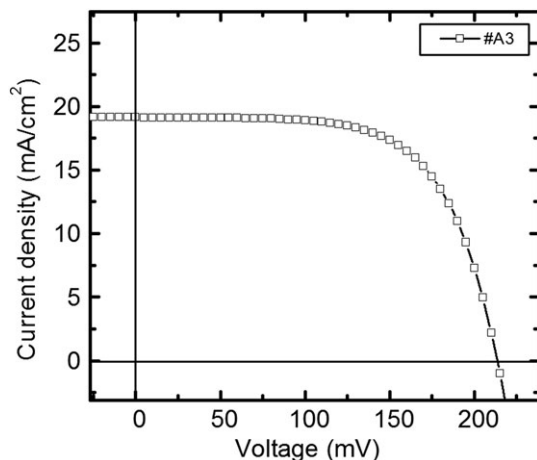


FIGURE 3 One-sun J-V curve of an as-grown solar cell

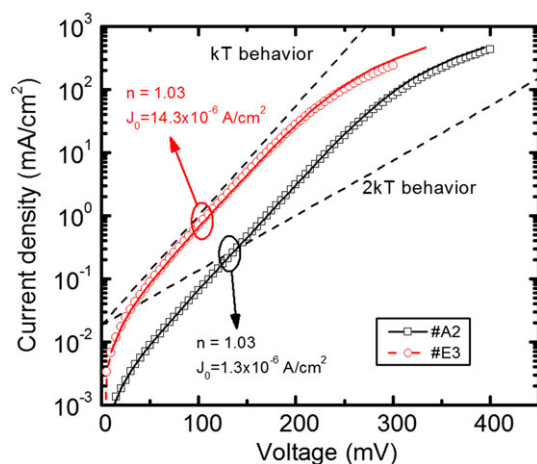


FIGURE 4 Dark J-V curve of representative as-grown and etched 3JSC Ge solar cells, plotted with black squares and red circles, respectively [Colour figure can be viewed at [wileyonlinelibrary.com](https://onlinelibrary.wiley.com/doi/10.1002/pip.2948)]

high currents. Indeed, an ideality factor of $n = 1$ is obtained from the fit of the curve made with a lumped analytical model. Similar dark J-V curves were obtained for the rest of the Ge solar cells with different wafer resistivity values. Because the ideality factor of these solar cells is $n = 1$, we can conclude that the recombination of carriers mainly takes place in the quasi-neutral regions.¹⁹

In turn, Figure 5 shows the averaged V_{OC} of the as-grown devices plotted (black squares) versus wafer resistivity. Besides, the experimental data are grouped according to the 2 different temperatures employed to grow the nucleation layer (empty and filled symbols for samples grown at 640 and 675°C, respectively). On the one hand, for the group grown at 640°C, there is no clear dependence with the resistivity of the wafer, which confirms that the V_{OC} mostly depends on the emitter properties.⁷ On the other hand, the sample grown at 675°C (#A3) shows a reduced V_{OC} as compared with the structure grown at 640°C (around 30 mV less).

As emitter thickness (X_E) may have a big influence on the V_{OC} of the Ge subcell,⁷ C-V electrochemical profiling measurements were performed on the Ge solar cells to estimate the electrical carrier concentration profile and X_E . Figure 6 shows the carrier concentration profiles of representative samples #A2 and #A3 (ie, similar wafer

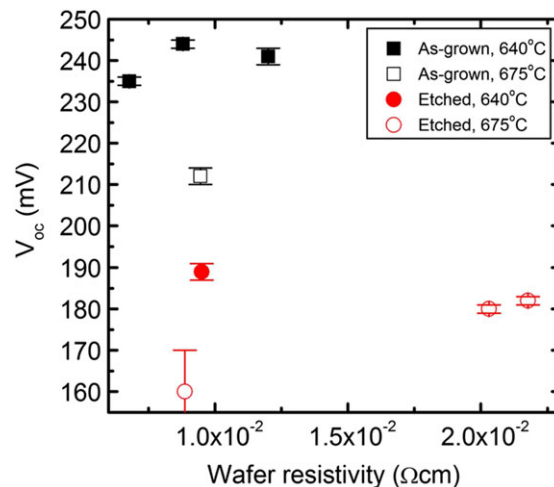


FIGURE 5 Averaged 1-sun V_{OC} of as-grown and etched 3JSC Ge solar cells, plotted with black squares and red circles, respectively. The full and open symbols represent samples with nucleation layer grown at 640 and 675°C, respectively [Colour figure can be viewed at [wileyonlinelibrary.com](https://onlinelibrary.wiley.com/doi/10.1002/pip.2948)]

resistivity and different nucleation temperature). The sample grown at 675°C (ie, sample #A3) shows a deep emitter, of around 250 nm, whereas the sample grown at 640°C (#A2) has a shallower emitter with a thickness between 160 and 190 nm. We also performed SIMS measurements on sample #A2 to check for P, Ga, and In contents and therefore shed some light on the diffusion processes taking place (Figure 7). On the one hand, P diffuses deep into the substrate creating the emitter. On the other hand, Ga and In diffusion is less pronounced but it will be taken into account later when discussing the particular shape of the CV profile.

3.2 | Etched triple junction solar cell solar cell characterization

The thermal load caused by the growth of the other subcells that constitute the MJSC structure significantly affects the performance of

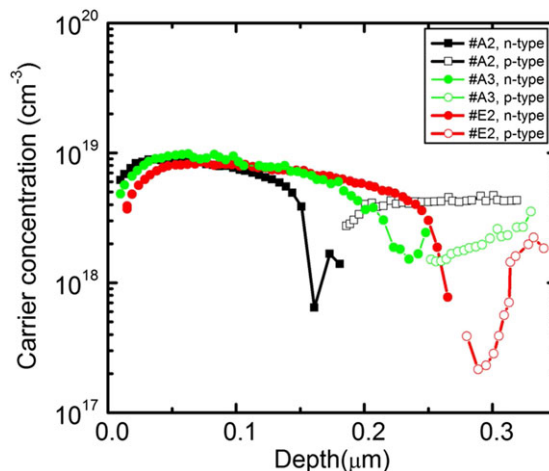


FIGURE 6 Carrier concentration profile of representative as-grown (black and green squares) and etched 3JSC Ge solar cell (red circles). The full and open symbols represent n-type and p-type doping, respectively [Colour figure can be viewed at [wileyonlinelibrary.com](https://onlinelibrary.wiley.com/doi/10.1002/pip.2948)]

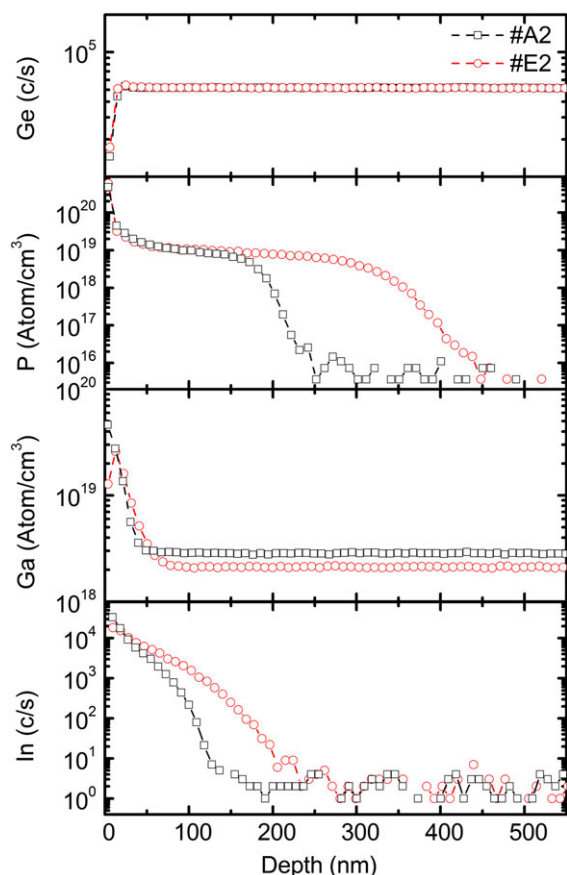


FIGURE 7 Secondary-ion mass spectroscopy (SIMS) measurements of Ge, P, Ga, and In elements of representative as-grown and etched 3JSC structures [Colour figure can be viewed at [wileyonlinelibrary.com](https://onlinelibrary.wiley.com/doi/10.1002/pip.2948)]

the Ge subcell. Figures 2B, 4, and 5 also show the performance of the etched 3JSC Ge solar cell devices, and Table 1 summarizes the averaged J_{SC} , V_{OC} , and FF values. In some cases, a higher variability in these values is obtained due to the final morphology of the remaining layers (where the electrical contacts are made) after the wet etching.

Figure 2B shows the IQE of the Ge solar cells after the growth of the 3JSC for a variety of wafer resistivity values as indicated in Table 1. Again, the absence of response in the range from 300 to 800 nm is due to the absorption that takes place in the GaInP nucleation and Ga(In)As layers that were not chemically etched away. In comparison with the IQE of the as-grown solar cells in Figure 2A, the IQE in the wavelength range between 900 and 1300 nm has decreased. As it will be shown later in the simulation section, a reasonably good fit of the curves can be obtained by assuming no contribution from the emitter region to the IQE, thus pointing out a significant degradation of the minority carrier properties in the emitter. This fact accounts for the significant drop in the IQE from 600 to 1200 nm, where the emitter response is the largest contributor to the device IQE. Besides, the IQE in the base region (that mostly shows from 1400 to 1700 nm) exhibits a slight dependence on the substrate resistivity, unlike the as-grown devices. The combination of these facts yields a reduction of the average 1-sun J_{SC} as observed in Table 1. However, due to the different optical thicknesses of the window and contact layers of the samples, the quantification of the current loss should be done by calculating the equivalent current loss obtained by the IQE difference between

etched and as-grown devices in the wavelength range from 950 to 1800 nm. In this way, we can account for up to 20% loss in J_{SC} .

Figure 4 also shows the dark I-V of sample #E3 (the lowest V_{OC} measured among the etched 3JSC devices is actually that of sample #E1, but we prefer not to discuss this value due to the high dispersion in the average V_{OC} value obtained). Such curve is similar to that of the as-grown device from #A2 and hence also shows 2 different regions, 1 influenced by series resistance and 1 with constant slope and ideality factor of $n = 1$. However, for the solar cell from structure #E3, the curve is shifted to lower voltages, which implies that there is an increase in the reverse saturation current density of etched 3JSC solar cells regarding the as-grown one of about 1 order of magnitude (from 1.4×10^{-6} to 1.5×10^{-5} A/cm²). In addition, no shunt resistance was observed in the solar cells analyzed in this work, neither in the as-grown nor in the etched 3JSC samples, which simplifies the EQE measurement of Ge subcells in 3JSCs.²⁰

The increase in the dark saturation current density observed will determine the V_{OC} of the device. Figure 5 shows with red circles the V_{OC} of the Ge devices after the growth of the TC and MC. Again, the data are split in samples with the GaInP nucleation layer grown at 675 and 640°C with filled and empty symbols, respectively. Each structure suffered a slightly different thermal load, as summarized in Table 1. Figure 5 shows that the V_{OC} of etched solar cells lie around 175 ± 15 mV, which represents an average ≈ 55 mV loss as compared with as-grown devices. As occurred with the as-grown samples, the V_{OC} seem largely unaffected by substrate resistivity.

To check the emitter properties and their eventual modification, C-V and SIMS profiles were also measured on etched 3JSC devices. Figure 6 shows the C-V measurement of an etched 3JSC device (structure #E2), which is directly comparable to structure #A2 (both with nucleation temperature of 640°C and similar substrate resistivity). Whereas the doping level of the emitter shows no significant change (within the measurement accuracy), the emitter depth X_E increases by 55% (from 180 to 280 nm). Besides, the shape of the doping profile in the emitter in the first 50 nm has changed as compared with the as-grown case, showing lower doping values. Secondary-ion mass spectroscopy measurements on an etched device on Figure 7 reveals that only P and In (and not Ga) diffuse further into the substrate during the growth of the whole MJSC, and therefore, a change in the C-V profile is expected.

4 | DISCUSSION

4.1 | Germanium emitter formation and evolution

Germanium emitter shows a characteristic, mesa-shape carrier concentration profile due to its formation by in-diffusion of P, Ga, and In during the GaInP layer growth (see Figures 6 and 7). Although Ga and In diffusion in Ge is, in principle, less intense than the diffusion of group V elements (their diffusion coefficients are 2 to 3 orders of magnitude lower than those of group V elements¹²), they affect the emitter free carrier concentration profile. Besides, results in Figures 6 and 7 show that the thermal load acts as a drive-in process that favors further P and In penetration into the substrate.

P atoms diffuse and create the n-type emitter by compensation of the p-type dopant of the substrate (Ga in the wafers used in this work), which explains the gradual transition from the uniform p-type doped substrate to the n-type plateau region in the C-V profile of Figure 6. Going from right to left in Figure 6, as P concentration increases, the effective p-type carrier concentration level is reduced until it switches to n-type and then smoothly increases until an uniform level is reached (ie, the n-type plateau we see in Figure 6). At this point, the emitter C-V carrier concentration profile approximately reproduces the SIMS P concentration profile, meaning that the ionization of P atoms is almost complete at room temperature. In addition, group III elements (such as Ga and In) also diffuse into the Ge substrate, acting as p-type dopants. Although a quantitative analysis was not possible because In was only given in counts/second in the SIMS measurement, it can be deduced that (i) In has a higher diffusion coefficient than Ga and (ii) group III diffusion coefficients are significantly lower than those of group V elements, in agreement with Dunlap.¹² The shallow diffusion of In and Ga creates an additional p-type doping close to the heterointerface that partially compensates the n-type P profile. However, as P diffusion in Ge shows a characteristic kink-and-tail profile,²¹ Ga and In compensations are not strong enough to revert to p-polarity, and they simply reduce the n-type concentration level obtained in the shallower region of the emitter. Hereafter, this region will be referred to as the *gradual emitter*. Finally, as shown in Figure 7, only P and In seem to diffuse further in Ge due to the extra thermal load. As a consequence, X_E is increased and the profile of the gradual emitter extends slightly deeper, as observed in Figure 6. The impact of both the thickness and the shape of the gradual emitter on the device performance will be assessed later, in the simulation section.

4.2 | Degradation of internal quantum efficiency and V_{OC} of etched devices

The degradation observed in the IQE of the etched 3JSC devices causes the photocurrent to drop. Although the current obtained in the etched 3JSC device (around 16.5 mA/cm², without ARC) is slightly overestimated as compared with the value we would have obtained in

a real MJSC (with the TC and MC absorbing part of the spectrum), it is still higher than the typical values needed for current matching with the TC and MC in a 3JSC under AM1.5D spectrum. This is probably the reason why this degradation has not been made evident because the Ge subcell will not limit the current of the whole 3JSC device in a monolithic, 2-terminal MJSC architecture. However, this fact should be taken into consideration in other multijunction architectures, such as upright metamorphic 3JSC or lattice-matched 4JSC,³ because a loss in photocurrent of the Ge BC would cause a loss in the photocurrent of the whole MJSC.

The degradation in the IQE is mainly observed in the emitter region. Figure 8 shows the simulated IQE of devices #A2 and #E3 (same devices as in Figure 4), together with the contributions of each part of the device. In both cases, the main contribution to the IQE comes from the base, and a slight degradation from that region can be seen in sample #E3. For as-grown devices, the emitter contributes little to the IQE (around 5% relative), whereas for etched devices, assuming there is no contribution at all from the emitter, the emitter yields the best fit to the experimental data. In connection with this, for as-grown devices, X_E is increased and the change in the shape of the doping profile (see Figures 6 and 7) probably implies a modification in the band diagram at the GaInP/Ge heterointerface. Besides, it is reasonable to expect the minority carrier lifetime in the emitter ($L_{h,E}$) to be low, mainly because of its high doping level (close to 1×10^{19} cm⁻³). Anyhow, the relative importance of thickness versus gradual emitter as the potential origin behind the IQE degradation observed will be analyzed with simulations in the following section.

Regarding the degradation in V_{OC} in the etched 3JSC devices, it can be explained by a combination of the reduction in J_{SC} and the increase of the reverse saturation current density (J_0). According to our simulations, the drop in J_{SC} only accounts for a loss of 4 mV in V_{OC} , while an increase of J_0 of about 1 order of magnitude (from 1.3×10^{-6} to 1.4×10^{-5} A/cm²) can account for as much as ≈ 60 mV, which combined agree quite well with the experimental data in Table 1. In the following section, we will use simulations to identify the different phenomena that could explain the observed increase in J_0 .

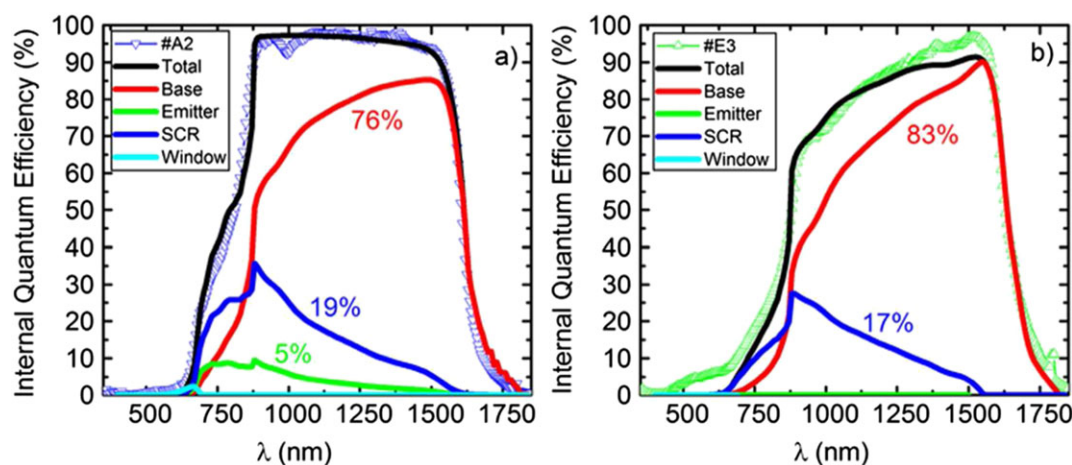


FIGURE 8 Experimental and simulated internal quantum efficiency (IQE) curves of samples #A2 (A) and #E3 (B), together with the contributions of each part of the device [Colour figure can be viewed at wileyonlinelibrary.com]

4.3 | Simulations

The reasons behind the degradation observed in both IQE and V_{OC} in etched 3JSC devices may be the change in X_E and/or the variation of the doping profile close to the III to V/Ge heterointerface (the gradual region), as experimentally observed in Figures 6 and 7. We also speculate that a change in the minority carrier diffusion length at the emitter ($L_{h,E}$) and in the nucleation/emitter interface recombination velocity (S_E) may have taken place. To identify or rule out the different mechanisms that may produce such degradation, we have performed simulations to determine (i) the impact of the gradual emitter shape and X_E and (ii) the influence of the minority carrier diffusion length at the emitter and S_E . The models and material parameters employed have been validated by simultaneously fitting the experimental IQE (by fitting independently the EQE and reflectance curves), light J-V, and dark J-V curves. Specifically, the data fitting routines were carried out for the same samples as in Figures 4 and 8 (#A2 and #E3). It is worth to mention that the simultaneous fit for sample #E3 is only achieved by including real doping profiles. Measured and simulated J-V parameters of devices #A2 and #E3 are in good agreement as summarized in Table 2. The highest deviation (4%) occurs for the J_{SC} values of device #E3, which is explained by the worse fitting of the IQE from 440 to 700 nm (see Figure 8).

4.3.1 | Impact of gradual emitter profile and emitter thickness

The electric field in a heterojunction between 2 different semiconductors results mainly from their band alignment, which can be modified by the doping level in each semiconductor. In the GaInP/Ge heterojunction that applies to this work, the particular doping profile created by the simultaneous diffusion of group V and III elements (ie, the so called gradual emitter) modifies the conduction and valence band in the vicinity of the heterointerface, as depicted in the simulation shown in Figure 9. This figure presents the conduction and valence band diagrams of an n-GaInP/n-Ge isotype heterojunction—calculated with ATLAS from Silvaco—for 3 cases, namely, the 2 doping profiles presented in Figure 6 and the ideal case of uniform doping. In other words, the band diagrams of Figure 9 represent those of solar cells #A2 and #E3 (as representative solar cells of as-grown and etched 3JSC devices, respectively) and a third case of constant doping included for comparison. As can be seen in the figure, a depletion region for electrons forms in the conduction band (Figure 9A), while an accumulation region for holes appears in the valence band in the Ge side next to the nucleation/emitter interface. Such regions become larger for cases where the gradual doping profile extends wider (eg, profile #E3). In the valence band, the accumulation region at the heterointerface confines minority carriers and pushes them toward the heterointerface where they readily recombine via interface states. In the conduction band, a

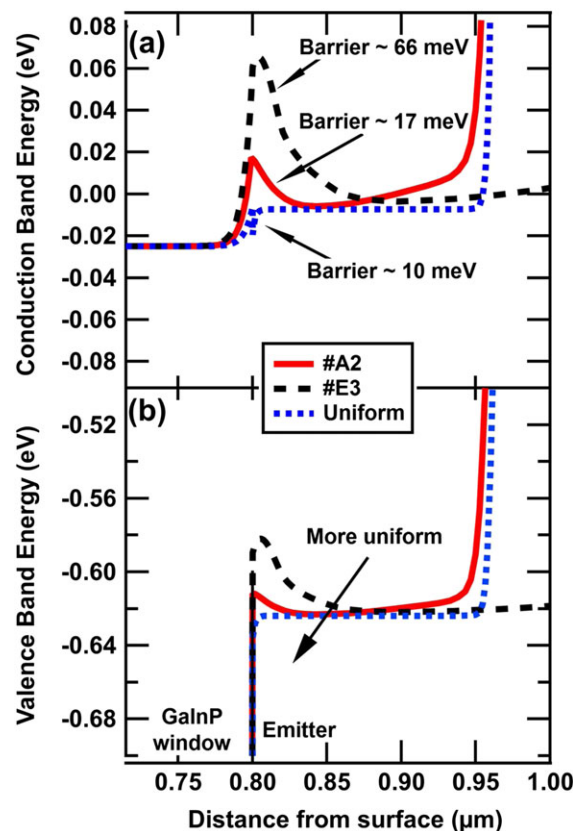


FIGURE 9 A, Conduction band energy at equilibrium for different emitter doping profiles measured. B, Valence band energy at equilibrium for different emitter doping profiles measured [Colour figure can be viewed at wileyonlinelibrary.com]

depletion region is formed by creating a potential barrier for majority carriers. Gudovskikh et al.¹³ suggested the presence of a p-type region between the GaInP window and the Ge emitter as the origin of the potential barrier of around 12 meV formed at their samples. In this work, we find that the gradient in the effective carrier concentration at the emitter interface is by itself enough to produce such barriers (ie, 17 meV for an as-grown sample).

To quantify the impact of these different band diagrams (structures #A2 and #E3) on the electrical performance of the Ge subcells, the corresponding J-V curves were simulated. As a first approach, the emitter minority carrier diffusion length and S_E values of structure #A2 ($0.6 \mu\text{m}$ and $1.5 \cdot 10^4 \text{ cm/s}$, respectively) were assumed for both structures. In this respect, this first simulation allowed us to assess the sole influence of the emitter characteristics (ie, doping gradient and thickness) in the V_{OC} of the devices. Under these assumptions, the difference in the calculated V_{OC} between profiles #A2 and #E3 was only 10 mV (247 and 237 mV, respectively), much less than observed experimentally (see Table 2). If the simulation is repeated with the same X_E (280 nm) in both cases, but keeping their corresponding

TABLE 2 Measured and simulated J_{SC} , V_{OC} , and FF of representative devices of structures #A2 and #E3

Sample	J_{SC} (mA/cm ²)			V_{OC} (mV)			FF (%)		
	Exp	Sim	Deviation	Exp	Sim	Deviation	Exp	Sim	Deviation
#A2	20.7	20.7	0.0%	245	244	0.4%	66.8	67.0	0.3%
#E3	17.0	16.3	4.1%	180	180	0.0%	60.5	60.8	0.5%

gradual emitter, it yields a 9 mV loss for V_{OC} . In summary, neither the increase in X_E nor the shape of the gradual emitter can fully explain the degradation in V_{OC} experimentally observed for etched 3JSC devices.

4.3.2 | Impact of S_E and minority carrier properties at the emitter

In addition to the emitter depth and doping profile, there are other phenomena associated with the diffusions taking place that may influence the collection properties of the emitter. To name the most relevant, we have (i) the formation/evolution of new surface states at the GaInP/Ge heterointerface, (ii) the widening of the hole accumulation region explained in Figure 9, and (iii) the increase in the concentration of defects or minority carrier traps in the emitter region. Effects (i) and (ii) would increase the effective surface recombination velocity at the emitter (S_E), whereas effect (iii) would reduce its minority carrier (hole) diffusion length ($L_{h,E}$).

Therefore, to explore how variations in S_E and $L_{h,E}$ affect the V_{OC} and J_{SC} of the Ge subcell, we calculated the contour maps included in Figure 10. To this end, we have divided the Ge solar cell into 3 regions, 2 to describe the emitter, and a third one to describe the base. The first region, namely, emitter #1, corresponds to the so-called gradual emitter zone in the emitter and extends from the GaInP/Ge interface down to the depth where the highest doping level is reached (ie, at the beginning of the plateau region in the C-V profile of Figure 6). This region essentially is the zone where the 3 diffusion profiles of Ga, In, and P coexist to influence the effective n-type doping in the germanium. The second region, namely, emitter #2, extends from the highest doping level to the junction depth (X_E). Analogously, this region essentially represents the zone of the plateau and tail in the doping

concentration where only the diffusion of P needs to be considered to explain the n-type doping in the Ge. Finally, the third region is a just a p-type Ge slab with constant doping, corresponding to the substrate.

To feed the simulations, realistic material parameters need to be calculated for each region. In the case of the first region (emitter #1 or gradual emitter), we can expect a severe degradation of the electronic properties due to the heavy dopant compensation (shown in the C-V and SIMS measurements in the previous sections). In our model, this region is simulated with a constant minority carrier diffusion length ($L_{h,E}$), which is the parameter swept in the maps of Figure 10. However, in emitter #2 and in the base of the Ge solar cell, a much lower degree of compensation is expected, and thus, analytical models for minority carrier properties have been used. At the frontier between emitter #1 and emitter #2, the same value for the $L_{h,E}$ is forced to ensure material parameters' continuity. In particular, expressions for the doping dependence of minority carrier lifetime were taken from Gaubas and Vanhellemont²² for both p-type and n-type Ge, while those for carrier mobilities were obtained from Prince.²³ The same equations were used for holes as majority (p-type base) and minority carriers (n-type emitter #2) because to our knowledge, no empirical data for hole properties in highly doped n-type germanium can be found in the literature. Noticeably, hole properties in emitter #2 will vary with depth due to the gradient in dopant concentration, whereas electron properties in the p-type base will be constant throughout. Finally, bandgap narrowing in the highly doped n-type emitter was also accounted for using the analytical expression obtained in Jain and Roulston.²⁴ Despite that this expression was derived for uniformly doped materials and thus its accuracy may be limited when working with varying doping profiles,²⁵ the good quality

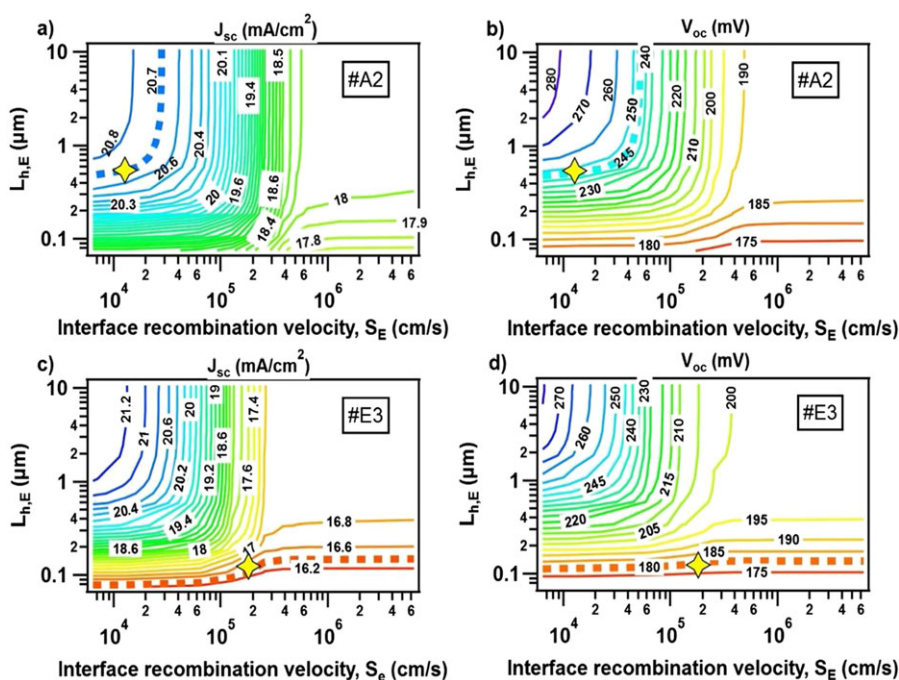


FIGURE 10 Simulated V_{OC} and J_{SC} as a function of S_E and $L_{h,E}$ of structures #A2 and #E3 with their corresponding emitter characteristics (ie, gradual emitter and thicknesses). The dashed thick lines indicate the range of values that fit experimental V_{OC} and J_{SC} independently, while the yellow star stands for the overlapping of the dashed thick lines corresponding to the best data fitting [Colour figure can be viewed at wileyonlinelibrary.com]

of the fits obtained back its applicability. Again, due to the doping profile in emitters #1 and #2, a variable bandgap narrowing versus depth is calculated in those layers, which, in turn, yields a variable bandgap across the emitter.

Figure 10A and B are contour plots of J_{SC} and V_{OC} , respectively, as a function of $L_{h,E}$ and S_E in emitter #1 for the as-grown device #A2. For this sample, the measured X_E was 180 nm, being the gradual emitter (emitter #1) 40 nm deep and the plateau-tail zone (emitter #2) 140 nm thick. The thick dashed lines in Figure 10A and B represent the iso- J_{SC} and iso- V_{OC} curves that match the experimental values measured for structure #A2 (see Table 2). Focusing on the current, in the iso- J_{SC} contour for 20.7 mA/cm² that applies to sample #A2, we have the following situation: the value of the minority carrier diffusion length stays fixed at $L_{h,E} \approx 0.5 \mu\text{m}$ for low values of S_E (horizontal stretch of the contour), whereas for high values of $L_{h,E}$, the surface recombination velocity stays fixed at $S_E \approx 3 \times 10^4 \text{ cm/s}$ (vertical stretch of the contour). In other words, in the horizontal stretch, the collection is limited by the value of the diffusion length and is insensitive to the low surface recombination velocity. In the vertical stretch, it is a high value of S_E that determines the amount of carriers lost at the surface (and thus collection) and $L_{h,E}$ has no impact because it has a value high enough to collect all remaining carriers. A similar discussion could be stated for V_{OC} maps in Figure 10B.

According to the latter explanation, an upper bound for S_E and a lower threshold for the $L_{h,E}$ can be established for sample #A2. Even more so, because the maps for J_{SC} and V_{OC} are calculated independently, the combinations of $L_{h,E}$ and S_E that fit the experimental J_{SC} and V_{OC} do not need to be exactly the same; ie, the thick dashed curves in Figure 10A and B do not exactly overlap. Therefore, the intersection between those curves represents the set of possible ($L_{h,E}$ and S_E) that have physical meaning for structure #A2. The overlap for the best fit occurs at the points marked with a yellow star in Figure 10A and B and allows to further reduce the range of S_E and $L_{h,E}$ ranges that fit the results of sample #A2.

Analogously, Figure 10C and D contains contour plots of J_{SC} and V_{OC} for the etched 3JSC device #E3, again as a function of $L_{h,E}$ and S_E . In this case, the additional thermal load produces an increase in X_E of about 100 nm, being the gradual emitter zone 90 nm deep, whereas the plateau-tail zone was of about 190 nm. Again, the thick dashed lines represent the iso- J_{SC} and iso- V_{OC} that match the experimental values measured for structure #E3 (see Table 2), and their overlapping corresponding to the best fit has been also marked with a yellow star. In this case, the iso- J_{SC} contour of 16.3 mA/cm² and the iso- V_{OC} curve of 180 mV that fit the experimental result do not look anymore as rounded corners but almost as flattened s-shaped curves or almost straight lines running parallel to the x-axis. This reveals an (almost) total insensitivity to S_E and a sole dependence on a very small diffusion length of $L_{h,E} \sim 0.14 \mu\text{m}$. In this way, the interpretation of the degradation process behind the thermal load is straightforward: a severe degradation of the minority carrier collection properties occurs in emitter #1.

All in all, the simulations show that hole properties of the n-type Ge emitter in the vicinity of the GaInP/Ge heterointerface are the main responsible for the recombination losses within the structure and are

limiting the V_{OC} of the devices. In fact, according to the simulations, the base accounts for just 16% of the total recombination losses for the as-grown case, whereas it drops to about only 3% for etched devices.

5 | SUMMARY AND CONCLUSIONS

During the growth of Ge-based MJSCs, the Ge subcell suffers performance degradation. To quantify this effect, we have grown and characterized single Ge solar cell test structures in the first place. These devices showed reasonably good V_{OC} (around 240 mV) and J_{SC} (around 19 mA/cm² without ARC) values, and there was no dependence of their IQE and V_{OC} with base doping.

Full triple-junction solar cells were grown subsequently (ie, adding 2 subcells, electrically connected with tunnel junctions, to the Ge solar cell structure), and then the 2 upper subcells—GaInP and Ga(In)As—were chemically etched to yield again a Ge single-junction cell, which realistically analyzes the impact of the thermal load on the Ge subcell performance. We observed a 20% and a 24% relative loss in equivalent J_{SC} and V_{OC} , respectively, together with a significant change in both the emitter depth and doping profile. The numerical modeling and simulation carried out unveiled an intricate effect of the thermal load on the interface and minority carrier parameters in this emitter. The IQE degradation and V_{OC} drop are mainly attributed to extremely poor minority carrier properties at the gradual emitter zone acting as an almost dead layer. This region is degraded to the point that becomes S_E independent in etched devices.

For MJSC architectures where the Ge subcell is highly current mismatched, a higher V_{OC} may be obtained if the thermal degradation is alleviated by means of using lower growth temperatures and/or lower growth times. In this way, X_E may be also reduced, which would enable better J_{SC} values. Alternatively, new nucleation routines should be explored to reduce (i) the formation of the gradual emitter due to indiffusion of group III elements, (ii) the interface recombination velocity at the emitter surface, and (iii) the carrier concentration value or the impact of a grown emitter with reduced doping value should be assessed.

ACKNOWLEDGEMENTS

This work has been supported by the European Commission through the LONGESST project (FP7 grant agreement no 607153), by the European Union's Horizon 2020 research and innovation program under the Marie Skłodowska-Curie grant agreement no 656208, by the Spanish Ministerio de Economía y Competitividad through the projects TEC2014-54260-C3-1-P and TEC2015-66722-R, and from the Madrid local government under contract S2013/MAE-2780 (MADRID-PV). I García is funded by the Spanish "Programa Estatal de Promoción del Talento y su Empleabilidad" through a Ramón y Cajal grant. The authors would also like to thank Jesus Bautista for his continuous support and NREL for the processing and facilities for the measurement of the solar cells. This paper reflects only the author's view, and the funding agency is not responsible for any use that may be made of the information it contains.

ORCID

Enrique Barrigón  <http://orcid.org/0000-0001-6755-1841>

Mario Ochoa  <http://orcid.org/0000-0003-4870-7390>

Ivan García  <http://orcid.org/0000-0002-9895-2020>

Laura Barrutia  <http://orcid.org/0000-0001-9363-6662>

Carlos Algora  <http://orcid.org/0000-0003-1872-7243>

Ignacio Rey-Stolle  <http://orcid.org/0000-0002-4919-5609>

REFERENCES

- Green MA, Emery K, Hishikawa Y, et al. Solar cell efficiency tables (version 49). *Prog Photovolt Res Appl*. Jan. 2017;25(1):3-13.
- King RR, Boca A, Hong W, et al. Band-gap-engineered architectures for high-efficiency multijunction concentrator solar cells. In: *24th European Photovoltaic Solar Energy Conference and Exhibition*. Vol. 21 Hamburg, Germany; 2009:55.
- Ochoa M, García I, Lombardero I, et al. "Advances towards 4J lattice-matched including dilute nitride subcell for terrestrial and space applications," in 2016 IEEE 43rd Photovoltaic Specialists Conference (PVSC), 2016, pp. 0052-0057.
- Barrigón E, Galiana B, Rey-Stolle I. Reflectance anisotropy spectroscopy assessment of the MOVPE nucleation of GaInP on germanium (1 0 0). *J Cryst Growth*. Jan. 2011;315(1):22-27.
- Galiana B, Barrigón E, Rey-Stolle I, et al. Compositional analysis and evolution of defects formed on GaInP epilayers grown on Germanium. *Superlattice Microsc*. Apr. 2009;45(4-5):277-284.
- He W, Lu SL, Dong JR, et al. Structural and optical properties of GaInP grown on germanium by metal-organic chemical vapor deposition. *Appl Phys Lett*. Sep. 2010;97(12):121909.
- Friedman DJ, Olson JM. Analysis of Ge junctions for GaInP/GaAs/Ge three-junction solar cells†. *Prog Photovolt Res Appl*. May 2001;9(3):179-189.
- Krut DD, Cavicchi BT, Lillington DR. "The development of Ge bottom cell for monolithic and stacked multi-junction applications," in The Conference Record of the Twenty-Second IEEE Photovoltaic Specialists Conference - 1991, 1991, pp. 90-92 vol.1.
- Li Y, Lazzarini L, Gilling LJ, Salviati G. On the sublattice location of GaAs grown on Ge. *J Appl Phys*. Nov. 1994;76(10):5748-5753.
- Tyagi R, Singh M, Thirumavalavan M, Srinivasan T, Agarwal SK. The influence of As and Ga prelayers on the metal-organic chemical vapor deposition of GaAs/Ge. *J Electron Mater*. Mar. 2002;31(3):234-237.
- Trumbore FA. Solid solubilities of impurity elements in germanium and silicon*. *Bell Syst Tech J*. Jan. 1960;39(1):205-233.
- Dunlap WC. Diffusion of impurities in germanium. *Phys Rev*. Jun. 1954;94(6):1531-1540.
- Gudovskikh AS, Zelentsov KS, Kalyuzhnyy NA, Evstropov VV, Lantratov VM, Mintairov SA. Interface properties of GaInP/Ge hetero-structure sub-cells of multi-junction solar cells. *J Phys D Appl Phys*. 2012;45(49):495305.
- Strobl GFX, Ebel L, Fuhrmann D, et al. "Development of lightweight space solar cells with 30% efficiency at end-of-life," in 2014 IEEE 40th Photovoltaic Specialist Conference (PVSC), 2014, pp. 3595-3600.
- Aho A, Tukiainen A, Polojärvi V, Guina M. Performance assessment of multijunction solar cells incorporating GaInNAsSb. *Nanoscale Res Lett*. Feb. 2014;9(1):61.
- Barrigón E, Rey-Stolle I, Galiana B, García I, Algora C. GaInP/GaInAs/Ge triple junction solar cells for ultra high concentration. In: *2009 Spanish Conference on Electron Devices*; 2009:383-386.
- "Device simulation software, 'Atlas User's Manual,' no. 408, pp. 567-1000." 2013.
- Baudrit M, Algora C. "Modeling of GaInP/GaAs dual-junction solar cells including tunnel junction," in 2008 33rd IEEE Photovoltaic Specialists Conference, 2008, pp. 1-5.
- Espinet-González P, Rey-Stolle I, Ochoa M, Algora C, García I, Barrigón E. Analysis of perimeter recombination in the subcells of GaInP/GaAs/Ge triple-junction solar cells. *Prog Photovolt Res Appl*. Jul. 2015;23(7):874-882.
- Barrigón E, Espinet-González P, Contreras Y, Rey-Stolle I. Implications of low breakdown voltage of component subcells on external quantum efficiency measurements of multijunction solar cells. *Prog Photovolt Res Appl*. Nov. 2015;23(11):1597-1607.
- Kobeleva SP, Anfimov IM, Yurchuk SY, Vygovskaya EA, Zhalnin BV. Influence of In_{0.56}Ga_{0.44}P/Ge heterostructure on diffusion of phosphorus in germanium during the formation of multiple solar cells. *Tech Phys Lett*. Jan. 2013;39(1):27-29.
- Gaubas E, Vanhellemont J. Dependence of carrier lifetime in germanium on resistivity and carrier injection level. *Appl Phys Lett*. Oct. 2006;89(14):142106.
- Prince MB. Drift mobilities in semiconductors. I. Germanium. *Phys Rev*. Nov. 1953;92(3):681-687.
- Jain SC, Roulston DJ. A simple expression for band gap narrowing (BGN) in heavily doped Si, Ge, GaAs and GeSi_{1-x} strained layers. *Solid-State Electron*. May 1991;34(5):453-465.
- Lowney JR, Bernnett HS. Effects of doping-density gradients on band-gap narrowing in silicon and GaAs devices. *J Appl Phys*. Jun. 1989;65(12):4823-4827.

How to cite this article: Barrigón E, Ochoa M, García I, Barrutia L, Algora C, Rey-Stolle I. Degradation of Ge subcells by thermal load during the growth of multijunction solar cells. *Prog Photovolt Res Appl*. 2018;26:102-111. <https://doi.org/10.1002/pip.2948>